13th AIAA/CIRA International Space Planes and Hypersonic Systems and Technologies Conference

Flight Data Analysis of HyShot 2

Neal E. Hass*, Michael K. Smart+
NASA Langley Research Center, Hampton, Virginia

Allan Paull!
University of Queensland, Brisbane, Australia

Abstract

The development of scramjet propulsion for alternative launch and payload delivery capabilities has comprised largely of ground experiments for the last 40 years. With the goal of validating the use of short duration ground test facilities, the University of Queensland, supported by a large international contingency, devised a ballistic re-entry vehicle experiment called HyShot to achieve supersonic combustion in flight above Mach 7.5. It consisted of a double wedge intake and two back-to-back constant area combustors; one supplied with hydrogen fuel at an equivalence ratio of 0.33 and the other un-fueled. Following a first launch failure on October 30th 2001, the University of Queensland conducted a successful second launch on July 30th, 2002. Post-flight data analysis of the second launch confirmed the presence of supersonic combustion during the approximately 3 second test window at altitudes between 35 and 29 km. Reasonable correlation between flight and some pre-flight shock tunnel tests was observed.

Nomenclature

f	aerodynamic factor
h	altitude
M	Mach number
P	pressure
q	dynamic pressure
s	seconds
T	temperature
V	velocity
w	mass flow
X	axial coordinate
Y	lateral coordinate
Z	normal coordinate
α	angle-of-attack
η_c	combustion efficiency
γ	ratio of specific heats
ϕ	equivelance ratio
ω	angular velocity about longitudinal body axis
ζ	angular velocity of longitudinal axis about velocity vector

* Aerospace Engineer, Hypersonic Airbreathing Propulsion Branch
+ Research Scientist, Hypersonic Airbreathing Propulsion Branch
! Professor, Mechanical Engineering Department

Subscripts:

0	freestream
c	combustor entrance
w	wedge
t2	Pitot

Introduction

The theoretical performance advantage of scramjets over rockets in hypersonic flight has been well known since the 1950's. For this reason, significant scramjet research has been conducted in many parts of the world[1]. Ground testing in continuous flow facilities has comprised most of the scramjet testing below Mach 8[2], whereas shock tunnels with flow durations of the order of 1-10 ms have been used for testing above Mach 7. The Centre for Hypersonics at the University of Queensland has routinely performed scramjet testing in shock tunnels for many years[3]. Based on the desire to validate such testing for conditions above Mach 7.5, a sounding rocket based flight test project known as HyShot was devised. This project involved two flight tests of a simplified supersonic combustion experiment designed solely through shock tunnel testing. While the HyShot scramjet payload was elegantly simple and quite robust, significant issues associated with providing suitable scramjet flight test conditions with the available rocket needed to be overcome. The chosen solution to these issues resulted in a highly parabolic trajectory, with the scramjet experiment being conducted during an almost vertical re-entry[4]. Some details of this novel approach are described in the paper, along with a discussion of how the trajectory was reconstructed solely from on-board measurements. Flight data analysis is then presented, along with comparison to some pre-flight ground test data.

Flight Profile Overview

Both HyShot flights took place at the Woomera Prohibited Area Test Range in central Australia. Each used a two-stage Terrier-Orion Mk70 rocket that generated a highly parabolic trajectory to boost the payload and the exhausted second stage Orion motor to an apogee in excess of 300km, as shown in Fig. 1. As the payload and attached second stage fell back to Earth, it reached a Mach number in excess of 7.5 between 35 and 25 km altitude, thus supplying a useful range of flight conditions for the testing of a scramjet. The almost vertical initial portion of this trajectory (the launch rail being at 77^{o}) lifted the payload quickly out of the atmosphere, therefore reducing both the payload/rocket heating loads and the integrated drag. This allowed for a relatively simple payload design, and a very high test Mach number for the combination of a Terrier-Orion booster and a 110kg payload. The main difficulty with this trajectory was the maintenance of stable flight upon re-entry into the atmosphere. This was successfully achieved through a re-orientation manoeuvre outside the atmosphere such that the payload re-entered nose first with a time varying attitude that produced payload angle-of-attack and yaw variations of approximately +/- 5 degrees during the scramjet experiment.

Payload Geometry

A schematic of the payload assembly is shown in fig. 2. It included a nose-cone to shroud the scramjet flowpaths on the initial ascent, two scramjet combustors orientated back-to-back on a wedge forebody, plus hydrogen and nitrogen tanks, batteries, telemetry system, flight computer and other components. One combustor was hydrogen fueled through 4 laterally spaced normal injectors, while the other combustor was unfueled so as to obtain baseline (tare) conditions to compare against the fueled flowpath throughout the flight. Figure 3 shows a photograph of the payload used for flight 2 (with the shroud removed). It was constructed predominantly of copper alloy for rapid dissipation of aerodynamic and combustion generated heat loads, with TZM used for the highest heat flux regions that occur at the leading edges of both combustors.

The goal of the experiment was to supply uniform flow into the two rectangular combustors at conditions ranging between Mach 7.2 and 8.0, allowing for an angle-of-attack (α) variation of the payload between +5 and -5 deg. In order to meet this goal and also to make the experiment as simple as possible, the flowpath intake was designed to allow significant flow spillage. As a further simplifying feature, the two flowpath nozzles were designed to exhaust laterally and generate very little overall thrust.

These characteristics, while not applicable to a practical scramjet where mass flow capture and thrust generation are to be maximized, eliminated risk factors associated with the intake and nozzle and enabled a simplistic supersonic combustion experiment to be conducted.

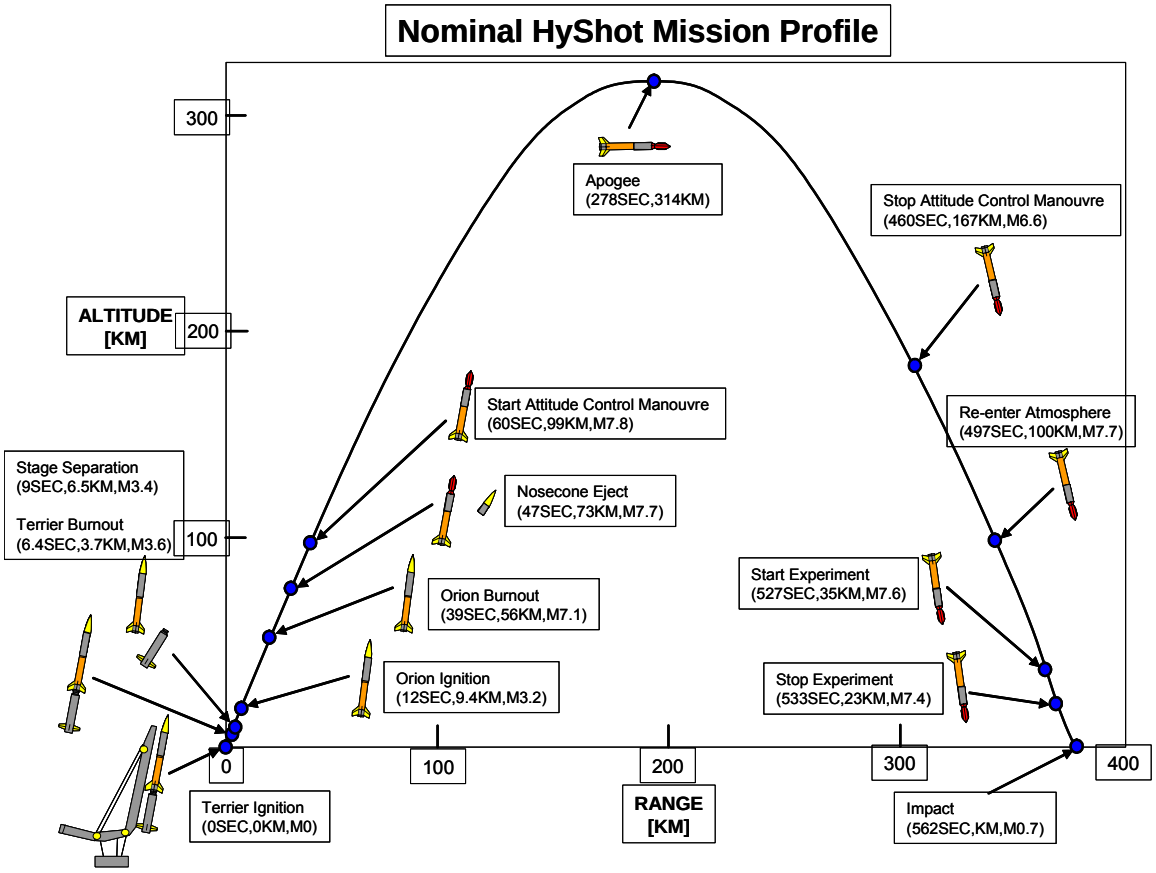

Figure 1. HyShot flight profile

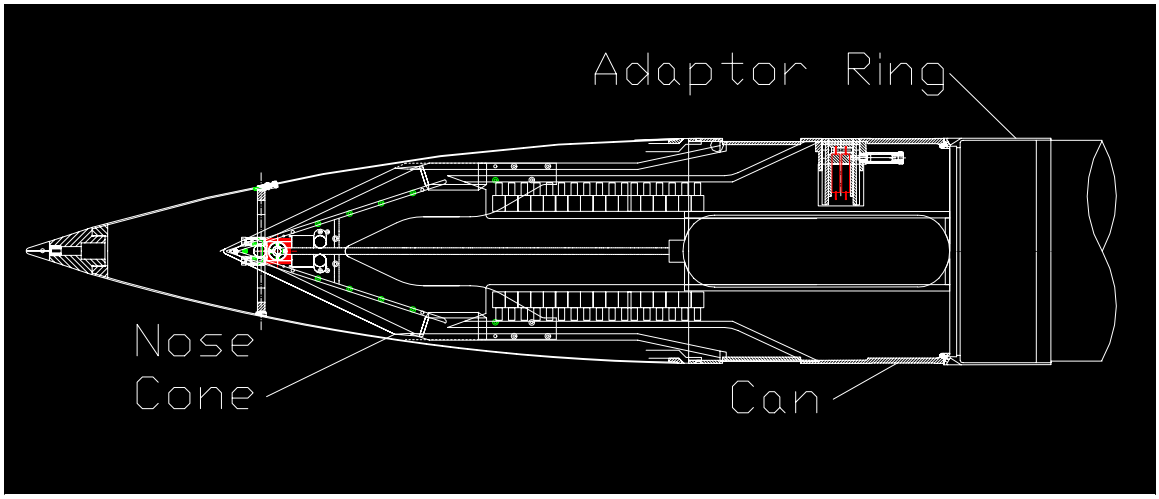

Figure 2. Schematic of the HyShot payload

Figure 3. HyShot payload

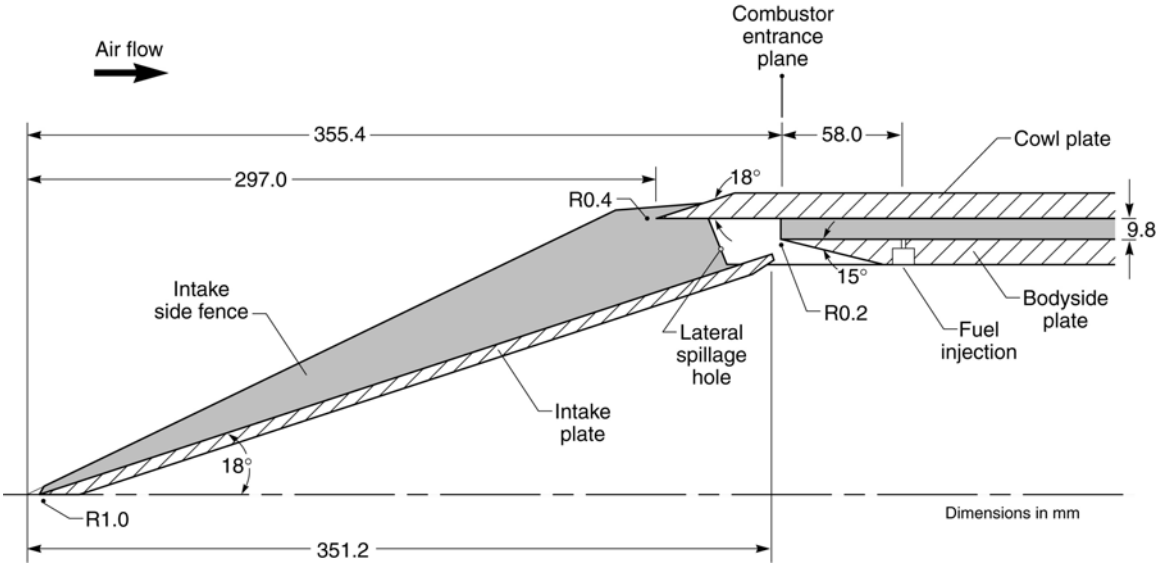

Figure 4. Schematic of Fueled flowpath

Figure 4 shows a schematic of the fueled flowpath. The intake consisted of a single 18 deg. wedge with a width of 100mm, a blunted leading edge, and highly swept side fences. The high wedge angle was necessary to ensure that the combustor entrance temperature and pressure were great enough to readily induce self-ignition of hydrogen. The rectangular combustor had a constant area 9.8 mm x 75 mm cross-section and a length of 300 mm (length/height = 30.61). The combustor cowl spanned the full width of the intake wedge and was situated such that the intake shock was upstream of its leading edge at all times. The flowpath design incorporated a shock trap that was situated between the end of the intake wedge and the entrance of the combustor. This feature not only captured the cowl shock, but also bled off the intake boundary layer. The reduced width of the combustor (relative to the intake wedge) and lateral spillage holes in the side fences adjacent to the shock trap were designed to remove the fence boundary layers and corner flows (see Fig. 5). The angle-of-attack of the payload is

defined as positive when the fueled combustor is on the windward side, and negative when the fueled combustor is leeward.

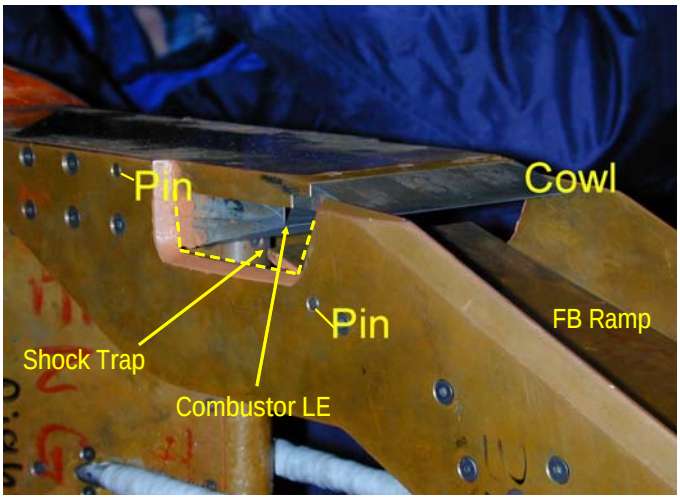

Figure 5. HyShot payload showing shock trap and lateral spillage holes

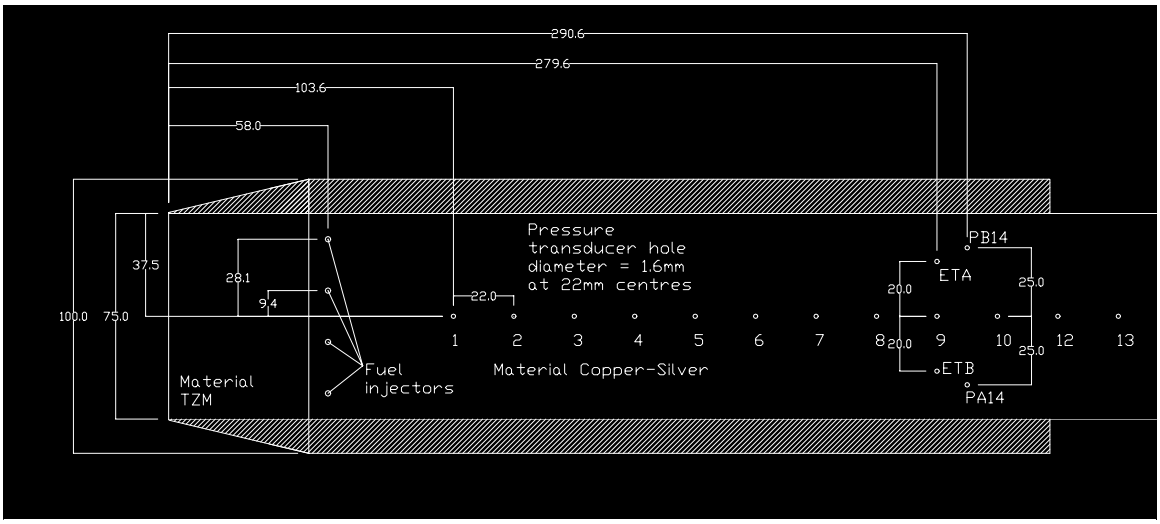

Figure 6. Combustor instrumentation layout and injector location (all measurements in millimetres)

Instrumentation

Instrumentation carried by the payload included pressure transducers, ceramic thermisters (thermo-resistors), thermocouples, accelerometers, magnetometers and horizon sensors. The onboard battery voltage was also measured. Fourteen pressure measurements were made along the bodyside wall of each combustor. Figure 6 displays the position of these measurements relative to the combustor entrance. The combustor entrance is defined as the axial position of the virtual leading edge of the bodyside combustor wall. Both combustor side walls began at this same axial position, while the cowl projected further forward. Thirteen of the pressure measurements were made on the centreline, beginning 103.6mm from the combustor entrance and continuing at 22 mm intervals. An additional measurement (labeled PA14 in the fueled combustor and PB14 in the un-fueled combustor) was made 25 mm away from the centreline, a distance 290.6mm from the combustor entrance. A single pressure measurement was also made on each intake wedge at a wetted distance of 59.4mm from the virtual

leading edge of the intake wedge and 3.6mm off the centreline. Unfortunately, the intake wedge surface pressure measurement for the unfueled combustor lagged that of the fueled intake wedge, and continually degraded as dynamic pressure increased. It is postulated that there was a leak in the transducer sensing line, hence this measurement was not used in the analysis.

All pressure transducers where mounted close to the back-side of each surface to provide a short response time. This was dictated by the expected 30% pressure variation every 70ms due to a payload spin rate in excess of 5 Hz and angle-of-attack variation between +5 and -5 degrees. However, the mounting point was also sufficiently far from the wall to provide for thermal protection of the transducers during the test window of the experiment. All transducers measured absolute values and were temperature compensated.

One temperature measurement was made on the back side of each of the bodyside combustor walls using a thermo-resistive sensor. These were located 279.6mm from the combustor entrance and 20mm off the centre-line, on the opposite side of the centerline to the 14th pressure transducer, and are denoted by ETA (ETB) in Fig. 6.

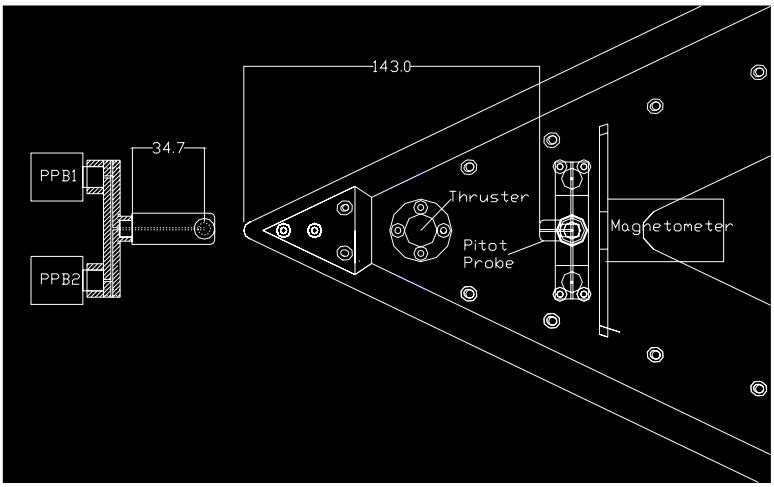

Figure 7. Payload leading edge showing Pitot probe and magnetometer location (all measurements in millimeters)

To determine free stream conditions during re-entry, two Pitot probes were mounted on either side of the intake each with two transducers attached in parallel, as indicated in Fig. 7. These transducers had different ranges so as to cope with the variations in atmospheric pressure during re-entry. The higher sensitivity gauges were appropriate for pressures up to 101kPa. The secondary set were used from 80kPa and above, and were linear to 350kPa.

Four accelerometers were mounted in the payload. Two measured the acceleration in the nominal direction of motion (x-axis) with different ranges and sensitivities. The other two measured the accelerations in two planes perpendicular to the nominal direction of motion (y and z-axis). The magnetometer and horizon sensor where utilized during the exo-atmospheric re-orientation manoeuvre.

All data was sampled approximately every 2ms, and a total of 48 analog and 4 digital channels were broadcast and recorded on the ground. There is no tracking data of the experiment trajectory due to a loss of radar lock immediately after the launch.

Fuel Supply System

The fuel used in the experiment was gaseous hydrogen. It was contained in a three litre tank with a maximum supply pressure of 21 MPa. The fueled flowpath was fed by four 0.2 mm diameter normal sonic injection ports 58 mm downstream of the combustor entrance on the bodyside (see Fig. 6). The pressure transducer used to control and monitor the fuel flow rate was mounted between the fuel control valve and the injectors. It had a range of 0-1.4Mpa and was temperature compensated. The fuel system was calibrated on the ground to determine a calibration constant between the measured fuel line pressure and the fuel mass flow rate. The hydrogen tank pressure and temperature were also monitored.

Fuel flow was triggered by and metered relative to the measured Pitot pressure. Pre-flight ground tests[5] had indicated that equivalence ratio's greater than 0.4 separated the boundary layer in the constant area combustor. For this reason, the metering valve was preset to maintain a fuel equivalence ratio of approximately 0.3 throughout the majority of the expected test window. Near the end of the experiment, the fueling was scheduled to increase in an attempt to unstart the fueled combustor.

Flight Test

The atmospheric conditions at Woomera for the July 30th, 2002 launch were near optimal. Launch site atmospheric pressure was just over 1000mb and there was no significant cloud cover. Balloon measurements indicated favorable conditions throughout the launch trajectory with atmospheric properties that very nearly matched 1976 standard atmospheric conditions. Ground temperatures at launch were near 15C with surface winds well below restriction limits. The launch proceeded with the test article clearing the rails without event (Fig. 8). Shortly after launch the launch site radar tracking station lost its lock on the telemetry and no tracking information was obtained. The downrange radar tracking station picked up telemetry radiation shortly after launch. Fortunately, coverage from both sources overlapped and telemetry for the whole trajectory was captured. Unfortunately, there was no radar tracking data to determine vehicle velocity and position.

Figure 8. Launch of HyShot 2

Trajectory Re-construction

Due to the failure of radar tracking, the HyShot 2 trajectory was reconstructed from on-board accelerometer, pressure transducer, magnetometer and horizon sensor measurements. The most detailed reconstruction to-date was performed by Qinetiq, a British organization which supported the project. This work is described in Ref. 6, and is the source for all trajectory information used in this paper.

The HyShot 2 flight trajectory may be broken into three phases; launch, space and re-entry. The launch phase involved the first stage Terrier burn, separation of the used Terrier motor, a second stage Orion burn, and blow off of the nose cone. This phase of the trajectory was reconstructed by integration of the axial accelerometer measurements, utilizing the assumption that the vehicle axis was aligned with the flight path. Based on this analysis, at t = 60.5 seconds after launch the payload/Orion motor (denoted as the "vehicle") was at an altitude of 99.25 km, a velocity of 2185.6 m/s, and a flight path angle of 69.7°. During the space phase of the trajectory the vehicle reached an apogee of 328.27 km and conducted a

re-orientation manoeuvre to produce a nose-down re-entry. The velocity, altitude and flight path angle for this phase of the trajectory were reconstructed using conservation of energy and momentum methods, and the change in vehicle attitude caused by the re-orientation was determined through magnetometer and horizon sensor measurements. Based on these analyses, the vehicle ended the space phase of the trajectory at t = 512.8 seconds at an altitude of 99.25 km, with a velocity of 2185.6 m/s and a flight path angle of -69.6°. The vehicle attitude at this stage of the trajectory varied with time as a result of a combination of roll and nutation. Roll is a rotation of the vehicle about its axis and nutation is a coning of the body axis about the velocity vector, as is shown in Figure 9. Based on the magnetometer and horizon sensor measurements, at the end of the space phase the vehicle was rolling at 5.2 Hz and nutating at an angle of 39° relative to the flight path. The angle-of-attack and yaw of the re-entering vehicle therefore undulated in a cyclic manner with amplitudes that varied with time.

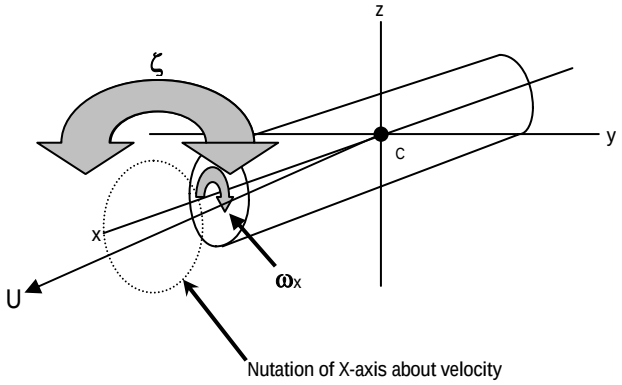

Figure 9. Schematic of a rolling and nutating body

The re-entry phase of the trajectory was re-constructed from integration of the axial accelerometer measurements, however this task was complicated by the fact that the vehicle axis was not aligned with the flowpath angle, and that the vehicle state at the end of the space phase was not known with sufficient accuracy to be used as an initial condition for re-entry integration. The effect of the vehicle attitude was accounted for by multiplying the axial acceleration measurements by a factor,

$$f = 1 + 0.1\alpha + 11.9\alpha^2 \qquad (1)$$

determined from aerodynamic testing of the vehicle described in Ref. 7. The time history of α needed to calculate f was determined from pressure measurements, as described later. An accurate estimate of the vehicle state at the start of the re-entry phase was determined by comparison with the measured Pitot pressure time histories. As described in Ref. 6, this process involved multiple trajectory integrations starting with a matrix of initial values for velocity and altitude (and the use of the 1976 standard atmospheric tables), to determine the combination that most closely matched the measured Pitot pressure history. This analysis (including the use of equation (1) for f) resulted in an initial state for the re-entry phase of the trajectory at an altitude of 99.25 km, as t = 508 seconds with a velocity of 2172.9 m/s and a flight path angle of -69.2°. No error estimation for these conditions has been made to date.

The goal of the flight was to fly a re-entry trajectory that supplied a multi-second window of flight at conditions appropriate for scramjet operation above Mach 7.5. Figure 10 shows the time histories of Mach number and dynamic pressure calculated using the re-constructed re-entry trajectory covering the period when the scramjet experiment took place. During this three second window, starting at t = 537.5 seconds, the Mach number remained between M = 7.75 and 8.0, which is slightly higher than the maximum value of 7.6 anticipated from pre-flight modeling of the trajectory. The observed jagged appearance of the Mach number time history during the experimental window is believed to be due to lack of conditioning of the accelerometer measurements. Figure 10 also shows that the dynamic pressure increased rapidly from q_0 = 21.0 to 58.5 kPa throughout the time window as the vehicle descended from an altitude of 34.9 to 28.1 km.

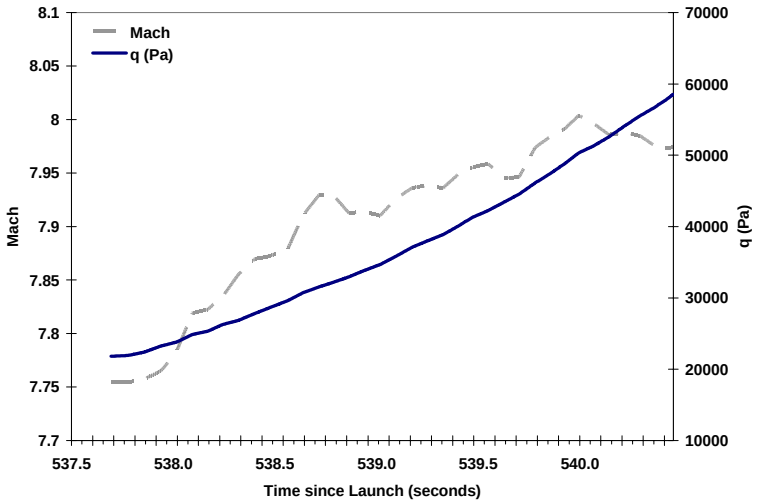

Figure 10. Reconstructed Mach number and dynamic pressure histories

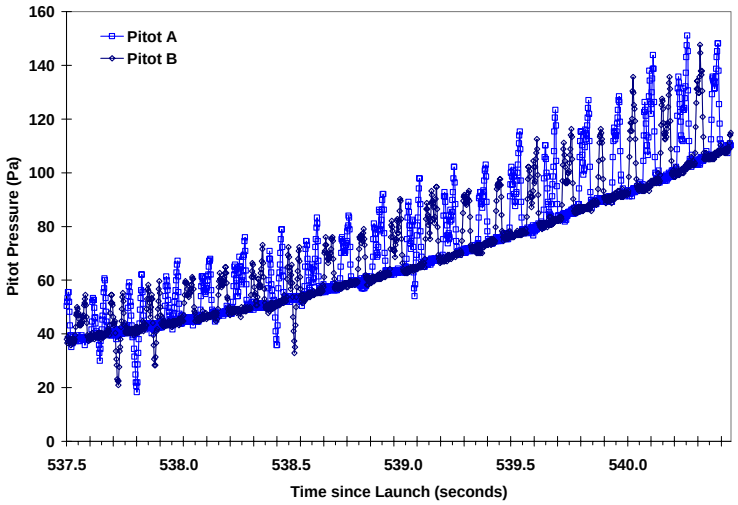

(a) Pitot pressure probe measurements

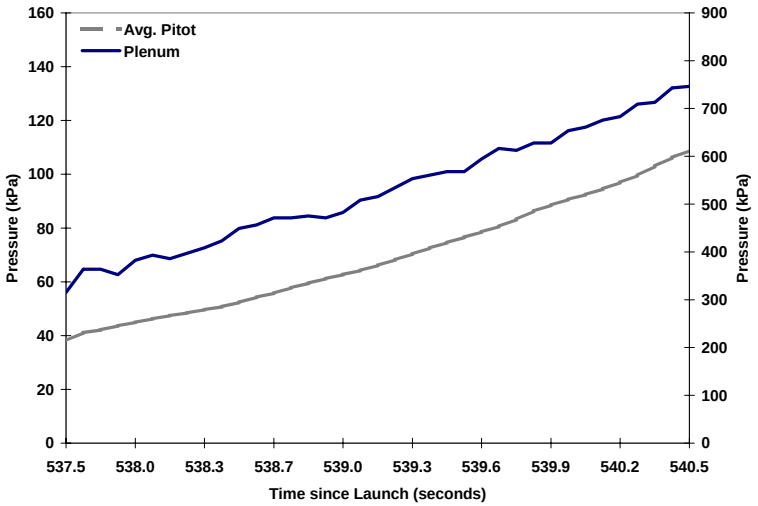

(b) Pitot pressure fit and fuel line pressure

Figure 11. Pitot pressure and fuel line pressure histories

Flight Data Analysis

Analysis of the flight data began with the two measured Pitot pressure histories, which are plotted in Fig. 11(a) over the three second test window beginning at t = 537.5 seconds. The first thing to note about these measurements is that while both Pitot pressures increased smoothly for portions of the time window, for other portions the Pitot pressures took periodic excursions to much higher levels. Also note that the excursions of the probes are out of phase with each other. Recalling that probes A and B are offset from opposite sides of the payload (Fig. 7), it is clear that this behavior is due to the roll and nutation of the vehicle, causing each probe to pass periodically behind the bow shock of the vehicle. The Pitot pressure time history that is applicable for flight data analysis is therefore represented by the smooth line shown in Fig. 11(b), which is an average of both probes measurements with the excursions removed. Also shown in Fig. 11(b) is the fuel line pressure history for the fueled combustor. As already discussed, hydrogen flow to the fuel injectors was designed to be initiated when the measured Pitot pressure crossed a pre-flight determined threshhold. The flight data indicated that this did in fact occur, with fuel flow commencing at t = 536.47 seconds at a time averaged Pitot pressure level of approximately P_{t2} = 34 kPa. In order to maintain a relatively constant ϕ, the fuel flow rate was metered to be proportional to the measured Pitot pressure.

The time history of the fueled intake wedge pressure is shown in Fig. 12. The undulations caused by the roll and nutation of the vehicle are evident in the figure. Examination of the time between peaks results in an estimate of the roll frequency during the experiment window of 6.25 Hz. Examiniation of a full nutation cycle results in an estimate of the nutation frequency during the experiment window of 1.6 Hz. Based on the geometry of the payload and these roll and nutation frequencies, the maximum rotational velocity of the payload is approximately 3 m/s; i.e. almost 3 orders of magnitude smaller than the total velocity of the vehicle, and is therefore inconsequential to the experiment.

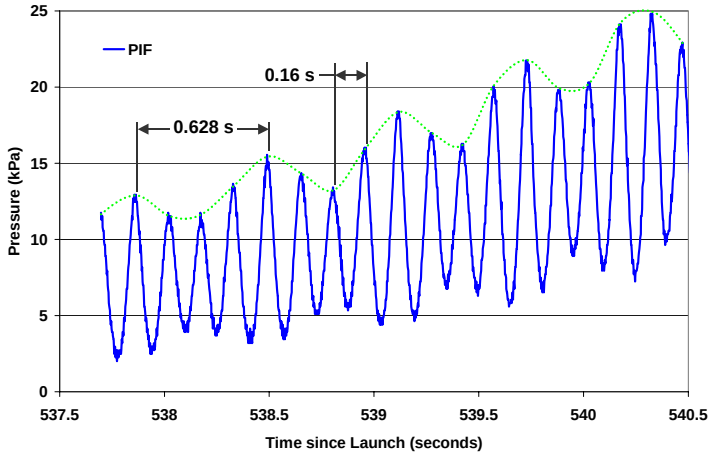

Figure 12. Intake wedge pressure history for the fueled combustor

As the vehicle rolled and nutated, its attitude cycled from time slices with the payload at zero yaw and the fueled side at positive α, through times with zero α and high yaw, to times with zero yaw and the fueled side at negative α. The time slices when the intake pressures were a maximum or a minimum correspond to when the intake wedges were at zero yaw. The time slices obtained when the intake pressure for the fueled combustor was a maximum corresponded to the maximum positive α for that cycle. These are referred to as windward time slices for the fueled combustor. Due to the back-to-back configuration of the two combustors, these time slices also corresponded to the minimum pressure on the intake of the un-fueled combustor, which are referred to as leeward time slices for the un-fueled combustor. In a similar manner, time slices obtained when the intake pressure for the fueled combustor was a minimum correspond to the maximum negative α, and are referred to as leeward conditions for the fueled combustor and windward conditions for the un-fueled combustor. Only data at time slices corresponding to zero yaw are examined in this paper.

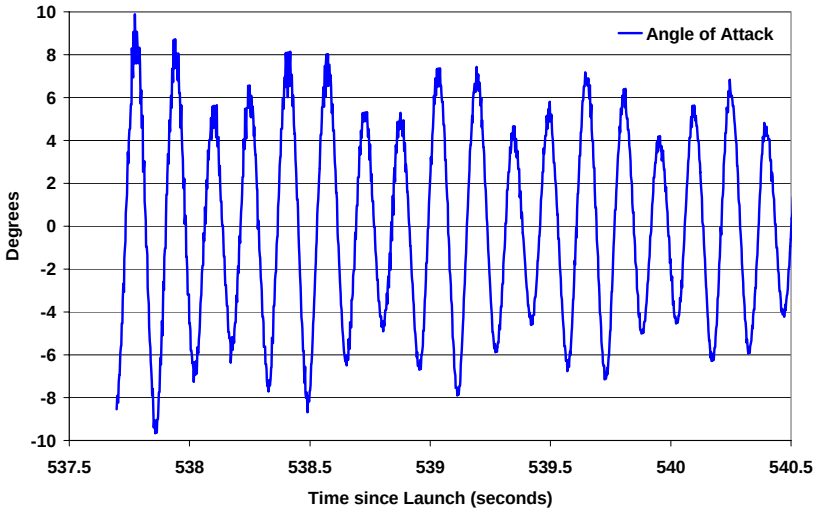

Figure 13. Vehicle angle-of-attack history

Vehicle angle-of-attack was determined using the Rankine-Hugoniot relations, which for a calorically perfect gas supply the following formula for the ratio of the intake wedge pressure and the Pitot pressure:

$$\frac{P_w}{P_{t2}} = \left\{ \frac{2\left[2\gamma M_0{}^2 \sin^2(18+\alpha) - (\gamma-1)\right]\left[(\gamma-1)M_0{}^2 \sin^2(18+\alpha) + 2\right]}{(\gamma+1)^2 M_0{}^2 \sin^2(18+\alpha)\left[(\gamma-1)M_0{}^2 + 2\right]} \right\}^{\frac{\gamma}{\gamma-1}} \quad (2)$$

The unknowns in equation (2) are α and M_0. However, this relation is insensitive to Mach number variations between M_0 = 7.5 and 8.0 (the range of interest in the time window of the experiment), and variations in γ due to thermal effects, therefore the time history of α was determined using a value of M_0 = 7.75 and γ = 1.40 in equation (2), and substitution of the measured time histories of the fueled intake wedge pressure and the Pitot pressure. Figure 13 shows the calculated α during the test window, clearly indicating the effects of both roll and nutation on the angle-of-attack experienced by the vehicle.

number	Time (s)	M_0	q_0 (kPa)	h (km)	α (deg.)
1	538.103	7.828	24.88	34.48	-5.012
2	538.179	7.831	25.33	34.31	5.540
3	538.734	7.938	31.55	33.05	-5.081
4	538.805	7.938	32.20	32.89	4.617

Table 1 – Flight parameters for analyzed time slices

Combustor Data Analysis

Analysis of the combustor data began with the choice of the most appropriate zero yaw time slices. The criteria used for this were; (i) q_0 > 23.94 kPa (500 psf), (ii) $\alpha < 6^o$ and (iii) as early as possible during the experimental window. Table 1 shows the flight parameters of the four time slices used for analysis in this paper. Combustor entrance properties were calculated for these four time slices, for both the fueled and un-fueled combustor, with the NASA Langley TPG code[8], which computes thermally perfect oblique shock flows. This was accomplished by processing the freestream flow through two oblique shocks. This calculation neglected losses associated with the bluntness of the wedge and combustor leading edges, and assumes no boundary layers enter the combustor. It will be seen in the following plots that this simplified analysis of the intake flow leads to an under estimate of the pressure ratio associated with the intake, but does allow normalization of pressure data to account for differences

associated with altitude and angle-of-attack. Table 2 lists the calculated combustor entrance conditions for the un-fueled combustor. Table 3 lists the calculated combustor entrance conditions for the fueled combustor, along with the equivalence ratio corresponding to the fuel flow rate measured at each time. As already noted, the fuel flow rate was metered relative to the measured Pitot pressure, and did not account for combustor mass capture variations caused by angle-of-attack variations. Despite this, equivalence ratio values at each of the time slices of interest varied by 6% and averaged ϕ = 0.33, slightly above the goal of ϕ = 0.3.

Number	Time (sec)	P_c (kPa)	T_c (K)	M_c	w (kg/s)
1	538.103	39.586	1305.9	2.604	0.1416
2	538.179	25.215	921.08	3.457	0.1440
3	538.734	50.53	1306.4	2.60	0.1713
4	538.805	34.13	943.5	3.39	0.1775

Table 2 – Entrance conditions for the un-fueled combustor

Number	Time (sec)	P_c (kPa)	T_c (K)	M_c	w (kg/s)	ϕ
1	538.103	25.567	936.97	3.414	0.1429	0.3331
2	538.179	40.994	1328.2	2.563	0.1430	0.3419
3	538.734	32.52	929.5	3.43	0.1725	0.3219
4	538.805	50.82	1287.0	2.636	0.1760	0.3254

Table 3 – Entrance conditions for the fueled combustor

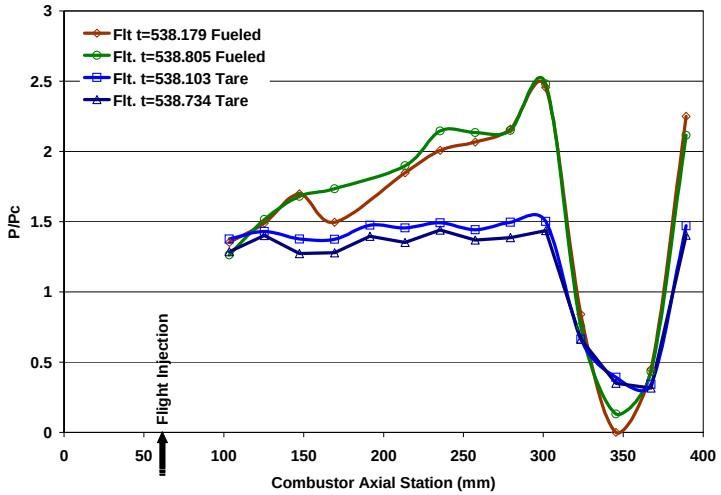

Figure 14. Windward fueled and un-fueled combustor pressure distributions

Figure 14 shows a comparison of the fueled and un-fueled combustor pressure distribution data for windward conditions. The data shown in the figure is normalized with the calculated combustor entrance pressure for each time slice, in order to remove differences associated with altitude and angle-of-attack. The un-fueled combustor pressure distributions show an average normalized pressure of 1.35 at the first pressure tap (103.6 mm along the combustor), and slowly increasing pressure, reaching a peak of 1.45 at the combustor exit. The high normalized pressure level of all the un-fueled combustor data (values closer to 1.0 would be expected) is a consequence of underestimating the intake pressure ratio. Whereas the steady increase in normalized pressure down the duct is due to boundary layer growth on the body, cowl and side walls. The fueled combustor pressure distributions have pressure level close to the un-fueled combustor for the first two pressure taps, before showing increased pressure rise due to hydrogen combustion by the third pressure tap (147.6 mm along the combustor). This indicates an ignition delay from the injection point at 58 mm along the combustor. By the combustor exit, supersonic combustion of hydrogen has raised the peak normalized pressure to 2.50, a pressure ratio of 1.85 relative to the first pressure tap (compared to a pressure ratio of 1.07 in the un-fueled combustor) A

pressure ratio of 1.78 can therefore be attributed directly to combustion of hydrogen. The significant drop in pressure observed at 320 mm along the combustor for both the fueled and un-fueled pressure distributions was due to the expansion fan emanating from the nozzle corner.

Figure 15 shows a similar comparison of fueled and un-fueled combustor pressure distributions for leeward conditions. In this instance the un-fueled combustor pressure distributions show an average normalized pressure of 1.32 at the first pressure tap, followed by a slowly increasing pressure that peaked at 1.55 at the combustor exit. The fueled combustor pressure distributions show greater pressure variations from shock waves than any of the other pressure distributions, but no clear effects of hydrogen combustion until 240 mm along the combustor. This indicates the presence of a significantly greater ignition delay than observed for windward conditions. Downstream of this point both fueled combustor time slices shown in Fig. 15 indicate a pressure rise due to supersonic combustion, however determination of a "typical" combustion generated pressure ratio is complicated by the presence of shock reflections in the duct. Averaging the values at the final combustor pressure tap for the fueled combustor time slices, supplies a nominal normalized pressure of 2.0. The pressure ratio for the fueled and un-fueled combustors, relative to the first pressure tap in the un-fueled combustor, was therefore 1.52 and 1.15, respectively, which corresponded to a pressure ratio due to combustion of 1.37 for leeward conditions. Based on these results, it is surmised that the higher Mach number and lower temperature and pressure of the leeward conditions led to less efficient combustion than occurred at windward conditions.

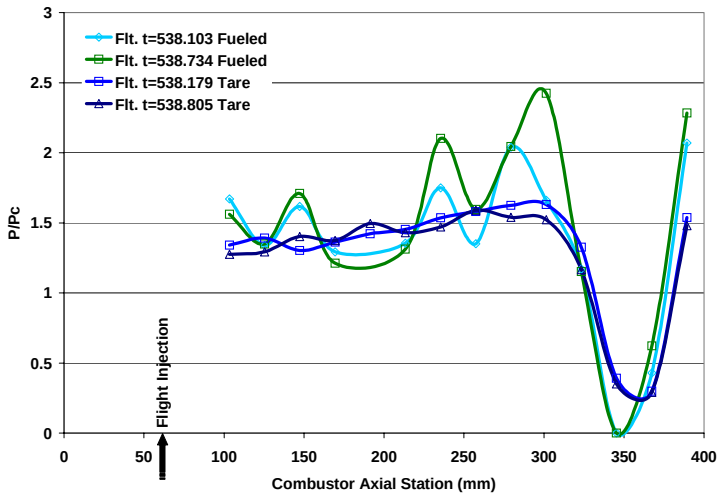

Fig. 15. Leeward fueled and un-fueled combustor pressure distributions

The flight data time slices chosen for analysis in this paper correspond to flight times before t = 539 s. This is due to a significant change in the character of the combustor data that was observed to occur at approximately t = 540 s. Figures 16(a) and (b) illustrate this change quite clearly for both windward and leeward conditions of the un-fueled combustor. Figure 16(a) shows normalized combustor pressure distributions for windward conditions at a series of zero yaw time slices between t = 538 and 541 s. Up to the t = 539.729 s time slice, the normalized combustor pressure distributions lay on top of each other, while after this time the normalized combustor pressure distributions are considerably higher. Based on these observations, it is postulated that at some time around t = 540 seconds, the un-fueled combustor underwent a geometrical change that generated significantly stronger shock waves in the combustor. The timing of this geometry change is further substantiated by similar plots of the leeward combustor pressure distributions shown in Fig. 16(b), which were significantly changed after t = 540.403 s.

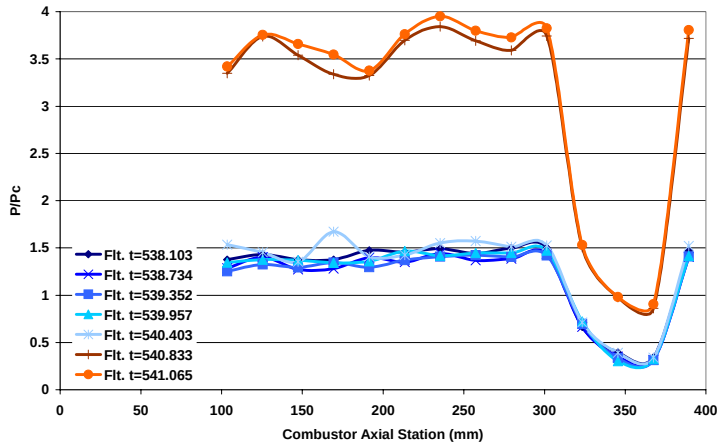

(a) Windward

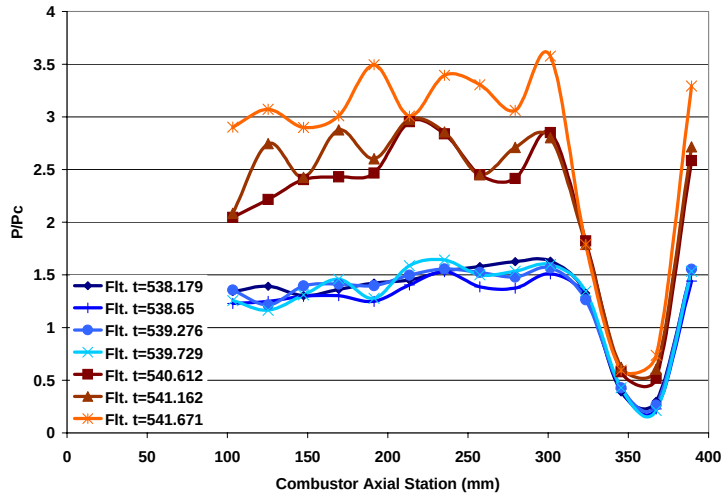

(b) Leeward

Figure 16. Combustor geometry divergence assessment

Flight to Ground Comparison

One of the important motivations for the HyShot flights was validation of short duration ground testing for scramjet development. As a first step towards this, a series of pre-flight shock tunnel experiments were conducted at the University of Queensland, to determine the expected performance of the flight payload. These experiments are documented in Ref. 5, and two hydrogen-fueled runs are compared here with the presented flight time slices. Further ground testing is planned with a model identical to that flown, and at conditions matching those experienced during the experimental flight window.

The model used for the pre-flight ground tests was designed to generate similar combustor entrance conditions to flight at Mach 7.6, while using an existing Mach 6.5 shock tunnel nozzle. This dictated the use of an experimental model with a 17° wedge intake (compared to 18° in the flight payload) and shock tunnel nozzle exit conditions with higher freestream pressure than flight. The 300 mm length combustor and fuel injectors were identical to flight, except that fuel injection took place 40 mm downstream of the combustor entrance (compared to 58 mm in flight), and the ground test model had an increased number of combustor pressure taps. A final difference between the ground and flight hardware was that the nozzle expansion was situated on the bodyside of the combustor for ground test (compared to the cowlside for the flight hardware). Table 4 lists the shock tunnel generated conditions used for comparison with flight. These two shock tunnel runs correspond to zero yaw flight data from the fueled

combustor at windward and leeward conditions. Table 5 lists the corresponding calculated combustor entrance conditions for the ground tests.

Run Number	M_0	P_0 (kPa)	T_0 (K)	q_0 (kPa)	α (deg.)
6857	6.456	3.012	337	87.878	4.0
6846	6.528	1.010	307	30.129	4.0

Table 4 – Ground test nozzle exit conditions

Run Number	M_C	P_C (kPa)	T_C (K)	w (kg/s)	ϕ
6857	2.6535	119.11	1311.6	0.4331	0.377
6846	3.2352	27.508	960.4	0.1438	0.476

Table 5 – Ground test combustor entrance conditions

Figure 17 shows a comparison between ground and flight data for the fueled combustor at windward conditions. Both ground and flight show a similar pressure rise due to supersonic combustion. However the flight data shows a higher peak pressure rise than the ground data, despite the fact that the ground test was fueled to a slightly higher equivalence ratio (ϕ = 0.377 compared with ϕ ~ 0.33 in flight). Figure 18 shows a comparison between ground and flight data for the fueled combustor at leeward conditions. Once again, both ground and flight data show a similar pressure rise due to supersonic combustion, with the ground data showing shorter ignition delay. Interpretation of these comparisons is hampered by the different axial positions of the pressure taps in the ground and flight models. More extensive comparisons will be made when the post-flight ground test data is available.

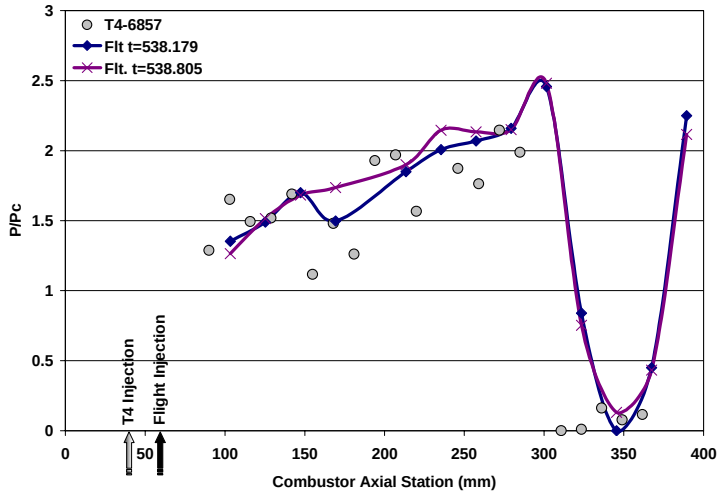

Figure 17. Flight-to-ground comparison for the fueled combustor at windward conditions

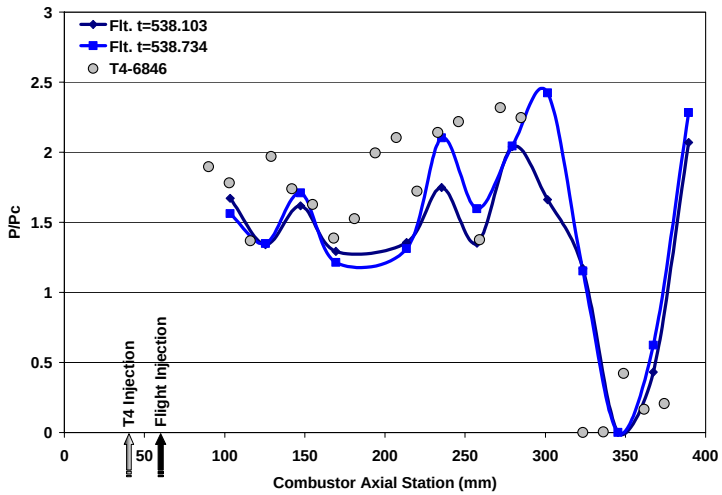

Figure 18. Flight-to-ground comparison for the fueled combustor at leeward conditions

Conclusions

A simple, but elegant, flight test experiment called HyShot was designed and flown above Mach 7.5 to validate the use of short duration ground test facilities for scramjet development. The scramjet payload was launched by an un-guided sounding rocket on a highly parabolic trajectory to an altitude in excess 328 km. The scramjet experiment was conducted during re-entry, and consisted of a double wedge intake with two back-to-back constant area combustion chambers, one fueled with hydrogen at an equivalence ratio of 0.33, and the other un-fueled. Trajectory analysis, reconstructed solely from on-board measurements, indicated that the scramjet payload underwent a combination of roll and nutation during reentry that generated payload attitudes varying between +/- 5 degrees angle-of-attack and yaw during the scramjet experiment.

Flight data analysis was conducted at time slices when the payload was at zero yaw conditions. The useful experimental time window lasted approximately three seconds, commencing 537.5 seconds after launch when the payload was slightly above 35 km altitude. The data indicated that hydrogen combustion generated a pressure ratio of approximately 1.78 for both windward conditions (angle-of-attack ~ 5 degrees, with Mach number ~ 2.6, temperature ~ 1330 K and pressure > 39 kPa at the combustor entrance), and 1.37 for leeward conditions (angle-of-attack ~ -5 degrees, with Mach number ~ 3.4, temperature ~ 930 K and pressure > 25 kPa at the combustor entrance). Based on these results, it appeared that the higher Mach number and lower temperature and pressure of the leeward conditions led to less efficient combustion than occurred at windward conditions. At approximately 540 seconds after launch, the pressure distributions in both the fueled and un-fueled combustors deviated from expected levels. This is believed to be due to the onset of mechanical failure of the payload. Comparison between flight and short duration ground tests conducted prior to the flight, demonstrated reasonable correlation. Further ground testing is planned at conditions close to those experienced during the experimental flight window.

Acknowledgement

The authors wish to thank Dr Terrence Cain of Gasdynamics Inc. for supplying the trajectory data used in this paper.

References

[1]Curran, E.T.,"Scramjet Engines: The First Forty Years", Journal of Propulsion and Power, Vol 17, No. 6., pp1138-1148, 2001.

[2]Guy, R.W., Rogers, R.C., Puster, R.L., Rock, K.E. and Diskin, G.S., "The NASA Langley Scramjet Test Complex", AIAA 96-3243, July, 1996.

[3]Paull, A., Stalker, R.J. and Mee, D.J, 1995, "Experiments on supersonic combustion ramjet propulsion in a shock tunnel", J. Fluid Mech vol 296 pp159-183.

[4]Paull, A., Alesi, H. and Anderson, S., “HyShot Flight Program and how it was developed”, AIAA 02-4939, September 2002.
[5]Paull, A., Frost, M. and Alesi, H., “HyShot-T4 Supersonic Combustion Experiments”, report for NAG-1-2113, 2000.
[6]Cain, T., Owens, R. and Walton, C., “Reconstruction of the HyShot 2 Flight from Onboard Sensors” Fifth Symposium on Aerothermodynamics for Space Vehicles, Cologne, Germany, November 2004.
[7]Owens, R. and Cain, T., “HyShot 2 Aerodynamics”, Fifth Symposium on Aerothermodynamics for Space Vehicles, Cologne, Germany, November 2004.
[8]Tatum, K.E., “Computation of thermally perfect properties of oblique shock waves”, NASA CR 4749, 1996.